Macromolecules

Article

pubs.acs.org/Macromolecules

Self-Healing Poly(acrylic acid) Hydrogels with Shape Memory Behavior of High Mechanical Strength

Umit Gulyuz and Oguz Okay*

Department of Chemistry, Istanbul Technical University, 34469 Maslak, Istanbul, Turkey

Supporting Information

ABSTRACT: A promising strategy to design synthetic hydrogels with the ability to self-heal is to substitute the covalently cross-linked polymer chains by supramolecular ones. Although supramolecular hydrogels generally exhibit rapid self-healing without the need for any stimulus, they suffer from low mechanical strength which prevents them from any stress-bearing applications. Here, we describe a novel way for the production of self-healing hydrogels with shape memory behavior of high tensile strength (0.7−1.7 MPa) and stretch at break (800−900%). Hydrophobically modified poly(acrylic acid) (PAAc) chains with cetyltrimethylammonium (CTA) counterions form the physical network of such hydrogels. They were prepared via micellar copolymerization of acrylic acid with 2 mol % stearyl methacrylate (C18) as the hydrophobic comonomer in an aqueous NaBr solution of cetyltrimethylammonium bromide (CTAB). Extraction of free CTAB micelles from the physical gels results in a drastic increase in their Young's moduli (from 8−30 to 180−600 kPa) and tensile strengths (from 0.1−0.2 to 0.7−1.7 MPa) due to the complex formation between PAAc and CTAB. Loading and unloading cycles conducted on hydrogels both at the state of preparation and at equilibrium in water show a significant hysteresis and good superposition of the successive loading curves, demonstrating damage done during loading is recoverable in nature. The hydrogel samples self-healed via heating and surfactant treatment of the damaged areas withstand up to 1.5 MPa stresses and rupture at a stretch of 600%. Because of the drastic change in the elastic modulus of PAAc hydrogels with a change in temperature, they also exhibit shape memory properties with a recovery ratio of 100%.

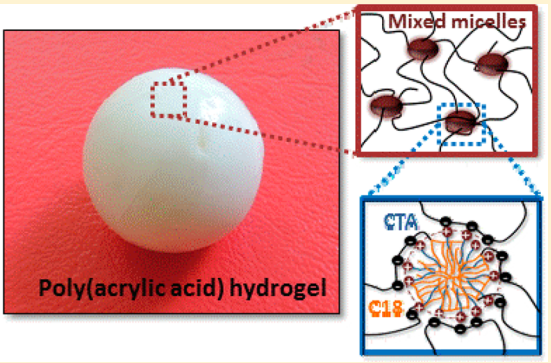

INTRODUCTION

Self-healing is one of the remarkable properties of biological materials such as skin, bones, and wood.[1,2] The ability of natural materials to heal cracks often involves an energy dissipation mechanism due to the so-called sacrificial bonds that break and re-form dynamically before the fracture of the molecular backbone.[3] Inspired by natural healing processes, a promising strategy to design synthetic hydrogels with the ability to self-heal is to substitute the covalently cross-linked polymer chains by supramolecular ones.[4−14] In the past few years, different reversible molecular interactions have been used to generate self-healing hydrogels, including hydrogen bonding,[15−19] electrostatic interactions,[20−22] molecular recognition,[23−25] metal coordination,[26,27] $\pi-\pi$ stacking,[28] dynamic chemical bonds,[29−32] molecular diffusion,[33,34] and hydrophobic associations.[35−39] Recently, we presented a simple strategy for the production of self-healing hydrogels via hydrophobic interactions.[35,36] Large hydrophobes such as stearyl methacrylate (C18) could be copolymerized with the hydrophilic monomer acrylamide (AAm) or acrylic acid (AAc) in aqueous sodium dodecyl sulfate (SDS) solutions. This was achieved by the addition of salt into the reaction solution. Salt leads to micellar growth and hence solubilization of large hydrophobes within the grown wormlike SDS micelles.[35] Incorporation of hydrophobic sequences within the hydrophilic polymer chains via micellar polymerization generates dynamic hydrophobic associations between the hydrophobic domains of polymer chains and surfactant micelles acting as physical cross-links of the resulting hydrogels. These reversible breakable cross-links are responsible for rapid self-healing of the hydrogels at room temperature without the need for any stimulus or healing agent.[35,36]

An important limitation of current methods to produce self-healing hydrogels is that they are not tailored toward ensuring a good mechanical performance at the same time. Self-healing hydrogels produced so far suffer from low mechanical strength which prevents them from any stress-bearing applications such as cartilage and tissue engineering scaffolds. To our knowledge, the magnitude of the tensile strength recovered after repairing for most healable hydrogels is below 0.4 MPa.[15−39] This mechanical weakness is due to the fact that the self-healing ability of a hydrogel is opposite its mechanical strength. For instance, the efficiency of self-healing increases with decreasing lifetime of dynamic cross-links due to the favorable chain

Received: July 23, 2014
Revised: September 9, 2014
Published: September 17, 2014

   dx.doi.org/10.1021/ma5015116 | Macromolecules 2014, 47, 6889−6899

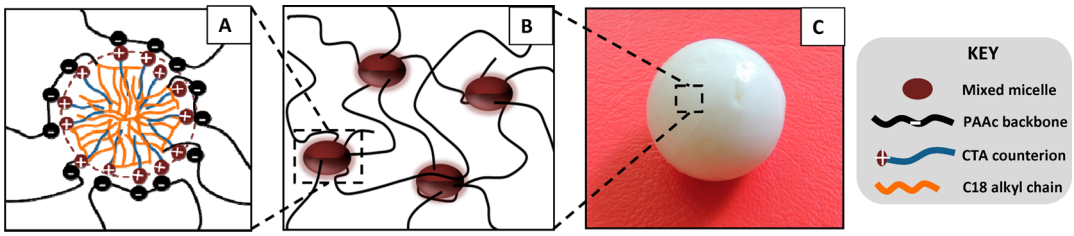

Figure 1. (A, B) Cartoon showing the cross-link in self-healing PAAc hydrogels. (C) Image of a PAAc hydrogel sample in the form of a sphere in equilibrium with water. C_0 = 20% and β_0 = 1/8.

diffusion across fractured surfaces of hydrogels. However, hydrogels with short-living cross-links necessarily become mechanically weak at experimental time scales. The challenge of producing self- or stimuli-healable hydrogels with a high mechanical strength is thus inherent.

A typical example for the antagonistic feature of self-healing ability to the mechanical strength is the hydrogel formed via hydrophobic interactions in a micellar solution.[36] Such hydrogels become mechanically strong upon their swelling in water, i.e., after extraction of surfactant micelles, due to the strengthening of hydrophobic associations without surfactant. However, they simultaneously lose their ability to self-heal due to the increased lifetimes of hydrophobic associations.[36] Here, we propose that self-healing hydrogels with improved mechanical properties could be obtained when the surfactant alkyl chains are trapped electrostatically in a supramolecular polymer network formed via hydrophobic interactions. Such physical networks can be generated from hydrophobically modified polyelectrolytes with oppositely charged surfactants via hydrophobic and electrostatic interactions. Figures 1A,B schematically depict this strategy. The mixed micelles acting as reversible cross-links are formed by the aggregates of polymer-bound surfactant alkyl cations and the hydrophobic blocks of the hydrophilic polymer. These physical cross-links will remain stable in water due to the electrostatic interactions between surfactant counterions and polymer backbone. Figure 1C shows the photograph of such a supramolecular hydrogel prepared in this study. In the following, we present self-healing hydrogels with shape memory behavior based on hydrophobically modified poly(acrylic acid) (PAAc) hydrogels with cetyltrimethylammonium (CTA) counterions of high tensile strength (0.7−1.7 MPa) and stretchability (800−900%).

The interactions of PAAc with an oppositely charged surfactant such as cetyltrimethylammonium bromide (CTAB) in aqueous solutions or gels has been extensively studied over the past 20 years.[40−47] The properties of such systems are determined by the parameter β, which is the molar ratio of surfactant to the acrylic acid (AAc) units in the polymer, i.e., β = [CTAB]/[AAc]. In dilute solutions, a single PAAc chain binds several CTAB micelles to form a complex, while at $\beta \cong 1$, the complex is saturated with surfactant.[40,43] The hydrodynamic radius of the complex is smaller than ($\beta < 1$) or similar to ($\beta > 1$) the radius of the surfactant-free PAAc coil.[43] Although the interactions between the fully ionized PAAc and CTAB is mainly electrostatic, hydrophobic interactions become increasingly important as the degree of ionization of PAAc is reduced.[40,43] The strength of the interactions increases after modification of PAAc chains with 1−3 mol % alkyl side chains.[48,49] It was shown that the cationic surfactant preferentially binds close to the alkyl groups of the hydrophobically modified PAAc in aqueous solutions and forms mixed micelles involving the alkyl groups of the polymer.[48]

In this study, we prepared physical PAAc hydrogels by copolymerization of AAc with 2 mol % C18 hydrophobe in aqueous CTAB solutions via the micellar polymerization technique. In this technique, developed by Candau and co-workers,[50−55] a water-insoluble hydrophobic comonomer solubilized within the micelles is copolymerized with a hydrophilic monomer in aqueous solutions by free-radical addition polymerization. Because of high local concentration of the hydrophobe within the micelles, the hydrophobic monomers are distributed as random blocks along the hydrophilic polymer backbone. The solubility of the large hydrophobe C18 in CTAB solution was provided by the addition of NaBr (0.25 M) which causes CTAB micelles to grow[56,57] and thus enables solubilization of C18 within the grown micelles. After copolymerization reactions and after equilibrium swelling in water, self-healing hydrogels with a β ratio between 0.065 and 0.120 were obtained where tensile strength and stretch at break after cut repairing can reach 1.5 MPa and 600%, respectively. To our knowledge, these values are the highest reported so far for self-healing hydrogels. Further, because of the drastic change in the elastic modulus of hydrogels with a change in temperature, the present hydrogels also exhibit shape memory properties with a recovery ratio of 100%. The synthesis strategy presented here could be extended to different hydrophilic and hydrophobic monomers as well as polyelectrolyte−oppositely charged surfactant systems to generate mechanically strong self-healing hydrogels with tunable properties.

EXPERIMENTAL PART

Materials. Acrylic acid (AAc, Merck) was freed from its inhibitor by passing through an inhibitor removal column purchased from the Aldrich Chemical Co. Commercially available stearyl methacrylate (C18, Aldrich) consists of 65% *n*-octadecyl methacrylate and 35% *n*-hexadecyl methacrylate. Cetyltrimethylammonium bromide (CTAB, Sigma), ammonium persulfate (APS, Sigma-Aldrich), sodium pyrosulfite ($Na_2S_2O_5$, Fluka), and sodium bromide (NaBr, Merck) were used as received. Stock solutions were prepared by dissolving 0.8 g of APS and 0.19 g of $Na_2S_2O_5$ separately in 10 mL of distilled water.

Determination of the Size of the Micelles. The measurements on CTAB solutions with and without the addition of NaBr, C18, and AAc were performed at 35 and 50 °C in the instrument Zetasizer Nano ZS from Malvern. The instrument contains a 4 mW He−Ne laser operating at a wavelength λ of 633 nm with a fixed detector angle of 173° and incorporates noninvasive backscatter optics. The data were analyzed by the cumulant method using Malvern application software, and the hydrodynamic correlation lengths ξ_H were obtained from the first cumulant.

Hydrogel Preparation. Micellar copolymerization of AAc with 2 mol % C18 was conducted at 50 °C in the presence of an APS (3.5 mM)−$Na_2S_2O_5$ (1 mM) redox initiator system in CTAB−NaBr

dx.doi.org/10.1021/ma5015116 | *Macromolecules* 2014, 47, 6889−6899

Table 1. Two Sets of Gelation Experiments Together with the Tensile Mechanical Properties of PAAc Hydrogels at the State of Preparation and in Equilibrium with Water[a]

					after preparation			in water		
C_0	β_0	β	W_g	$m_{rel,eq}$	E (kPa)	σ_f (MPa)	λ_f	E (kPa)	σ_f (MPa)	λ_f
15	0.125	0.089	0.97	0.39	8 (2)	0.10 (0.01)	35 (3)	183 (41)	0.71 (0.15)	9 (1)
20	0.125	0.088	0.96	0.37	16 (3)	0.15 (0.03)	27 (1)	307 (42)	1.05 (0.14)	9 (1)
30	0.125	0.085	0.97	0.52	47 (10)	0.20 (0.01)	23 (1)	515 (107)	1.28 (0.20)	10 (1)
30	0.100	0.065	1.00	0.68	42 (11)	0.26 (0.06)	24 (2)	295 (80)	1.14 (0.24)	10 (2)
30	0.125	0.085	0.97	0.52	47 (10)	0.20 (0.01)	20 (3)	515 (107)	1.28 (0.20)	10 (1)
30	0.167	0.120	0.95	0.48	30 (5)	0.12 (0.01)	19 (1)	605 (20)	1.66 (0.24)	10 (1)

[a] C_0 = initial monomer concentration (in % w/v). β_0 and β = CTAB/AAc molar ratio in the feed and in the polymer, respectively. W_g = gel fraction. $m_{rel,eq}$ = equilibrium relative weight swelling ratio in water. E = Young's modulus, σ_f = fracture stress, and λ_f = stretch at break. Standard deviations are given in the parentheses, while for the values of β, W_g, and $m_{rel,eq}$, they are less than 5%. The uniaxial compression test results are given in Table S1.

solutions. NaBr concentration was fixed at 0.25 M. The initial pH of the reaction solutions was 1.5 so that AAc is mostly protonated.[58] A summary of the experimental parameters and the characteristic data of the resulting gels are listed in Table 1. Two sets of gelation experiments were carried out. In the first set, the molar ratio β_0 of CTAB to AAc in the feed was set to 1/8 while the total monomer (AAc + C18) concentration C_0 was varied between 15% and 30% w/v. In the second set, C_0 was fixed at 30% w/v while β_0 was varied between 1/10 and 1/6. Depending on C_0 and β_0, CTAB concentration in the gelation solutions was between 0.24 and 0.64 M. The hydrodynamic correlation length ξ_H of these solutions was measured as 0.6 ± 0.1 nm, which increased to 6 ± 2 nm after addition of 0.25 M NaBr (Figure S1), indicating that CTAB micelles grow bigger. The growth of the micelles was accompanied by solubilization of up to 80 mM C18, which suffices to conduct the micellar copolymerization of AAc with 2 mol % C18 at a total concentration of 15−30% w/v.

To illustrate the synthetic procedure, we give details of the preparation of hydrogels at C_0 = 30% w/v and β_0 = 1/8. CTAB (1.7383 g) was dissolved in 6.5 mL of 0.25 M NaBr at 35 °C to obtain a transparent solution. After bubbling nitrogen, C18 (0.2556 g) was dissolved in this CTAB−NaBr solution under stirring for 5 h at 35 °C. After addition and dissolving AAc (2.744 g) for 30 min, stock solutions of $Na_2S_2O_5$ (100 μL) and finally APS (100 μL) were added to initiate the reaction. A portion of this solution was transferred between the plates of the rheometer to follow the reaction by oscillatory small-strain shear measurements. For the gel fraction determination and for the mechanical measurements, the remaining part of the solution was transferred into several plastic syringes of 4.8 mm internal diameter and the polymerization was conducted for 1 day at 50 °C. For rheological characterization of equilibrium swollen gel samples, polymerization reactions were also carried out between two glass plates (5 × 5 cm) separated by a 0.5 mm Teflon spacer. For preparation of gels in the form of spheres, gelation reactions were carried out in spherical plastic molds 5 cm in diameter.

Rheological Experiments. Gelation reactions were carried out at 50 °C within the rheometer (Gemini 150 Rheometer system, Bohlin Instruments) equipped with a cone-and-plate geometry with a cone angle of 4° and a diameter of 40 mm. The instrument was equipped with a Peltier device for temperature control. During all rheological measurements, a solvent trap was used to minimize the evaporation. An angular frequency ω of 6.3 rad s^{-1} and a deformation amplitude γ_0 of 0.01 were selected to ensure that the oscillatory deformation is within the linear regime. After a reaction time of 1 h, the dynamic moduli of the reaction solutions approached limiting values (Figure S2). Then, frequency-sweep tests were carried out at 25 °C, as described before.[36] The rheological behavior of hydrogels in equilibrium with water was determined using the gel samples prepared in the form of sheets that were extracted with water as detailed in the next section. To obtain hydrogels at various water contents w_{H_2O}, swollen gel samples were placed in sealed 50 mL—vials at room temperature to evaporate a desired amount of the gel water. This procedure ensured uniformity of the polymer concentration throughout the gel sample.[59] After a given evaporation time (a few minutes up to a few weeks), the masses of partially swollen gels were measured, from which their water contents were calculated. The thermal behavior of the hydrogels was investigated by first keeping the samples at 80 °C and then cooling down to 5 °C, after keeping for 10 min at 5 °C and heating back to 80 °C. The cooling/heating steps were carried out at a fixed rate of 1 °C/min. The changes in the dynamic moduli of gels were monitored during the course of the cycle as a function of temperature at ω = 6.3 rad s^{-1} and γ_0 = 0.001.

Swelling and Gel Fraction Measurements. Cylindrical hydrogel samples (diameter 4.8 mm, length about 2 cm) or hydrogel samples in the form of sheets of approximately 0.5 mm in thickness were immersed in a large excess of water at 23 ± 2 °C for at least 15 days by replacing water every day to extract any soluble species. Since pH inside the gel is equal to 1.5 at the state of preparation, upon immersion of the gel samples in water, pH increases from 1.5 to 6.7, leading to the onset of complexation between PAAc and CTAB and, hence, shrinking of the gel (see below). The mass m of the gel samples was monitored as a function of swelling time by weighing the samples. The relative mass m_{rel} of gels with respect to the after preparation state was calculated as $m_{rel} = m/m_0$, where m_0 is the initial mass of the gel sample. Then, the gel samples in equilibrium with pure water with a relative gel mass $m_{rel,eq}$ were taken out of water and freeze-dried. The gel fraction W_g, that is, the conversion of monomers to the cross-linked polymer (mass of water-insoluble polymer/initial mass of the monomer), was calculated from the masses of dry polymer network and from the comonomer feed. Swelling measurements were also conducted in aqueous solutions of various pH values between 1 and 12 adjusted by adding either HCl or NaOH solutions.

For the determination the amount of bound CTAB to PAAc network chains, freeze-dried gel samples were subjected elemental analysis measurements using a Thermo Flash EA-1112 Series elemental analyzer. From the nitrogen contents of the dried gels, the molar ratio β of CTAB to AAc units in the polymer was calculated (Table S2). DSC measurements were conducted on a PerkinElmer Diamond DSC under a nitrogen atmosphere. The gel samples sealed in aluminum pans were scanned between 5 and 80 °C with a heating and cooling rate of 5 °C/min.

Mechanical Tests. Uniaxial compression and elongation measurements were performed on cylindrical hydrogel samples after synthesis (4.8 mm diameter) and after equilibrium in water in a thermostated room at 24 ± 1 °C on a Zwick Roell test machine. Load and displacement data were collected during the experiments. The stress was presented by its nominal σ_{nom} or true values σ_{true} (= $\lambda\sigma_{nom}$), which are the forces per cross-sectional area of the undeformed and deformed gel specimen respectively, while the strain is given by λ, the deformation ratio (deformed length/initial length). The fracture stress σ_f and the deformation λ_f at break were recorded. The Young's modulus E was calculated from the slope of stress−strain curves between deformation of 5% and 15%.

Uniaxial compression measurements were performed using a 500 N load cell. Before the test, an initial compressive contact to 0.01 ± 0.002

dx.doi.org/10.1021/ma5015116 | Macromolecules 2014, 47, 6889−6899

N was applied to ensure a complete contact between the gel and the plates. Paraffin oil was used as lubricant to reduce friction and adhesion between the plates and the gel surface. We have to mention that the gel samples both after preparation and in equilibrium with water did not break even at a strain of about 100% compression, and therefore, the nominal stress σ_{nom} increased continuously with increasing strain (Figure S3). However, the corresponding $\sigma_{true}-\lambda$ plots pass through maxima indicating the onset of failure in the gel specimen (Figure S3). This behavior is likely a result of the self-healing ability of the hydrogels;[60] the samples breaking into several pieces still support the stress. Therefore, the fracture nominal stress σ_f and stretch λ_f at failure were calculated from the maxima in $\sigma_{true}-\lambda$ plots. Cyclic tests were conducted with a compression step performed at a constant cross-head speed of 5 mm/min to a maximum load, followed by immediate retraction to zero displacement and a waiting time of 5 min, until the next cycle of compression.

Uniaxial elongation measurements were performed using 10 and 500 N load cells under the following conditions: cross-head speed = 5 and 50 mm min^{-1} for $\lambda < 1.15$ and $\lambda > 1.15$, respectively; sample length between jaws = 11 ± 1 mm. Cyclic elongation tests were conducted at a constant cross-head speed of 50 mm min^{-1} to a maximum elongation ratio, followed by retraction to zero force and a waiting time of 5 min, until the next cycle of elongation. For reproducibility, at least six samples were measured for each gel and the results were averaged.

Self-Healing Behavior. To quantify the healing efficiency, tensile testing experiments were performed using virgin and healed cylindrical gel samples of 4.8 mm diameter and 6 cm length. The virgin gel samples after synthesis and in equilibrium with water were cut in the middle, and then the two halves were merged together within a plastic syringe (of the same diameter as the gel sample) by slightly pressing the piston plunger. For the hydrogels after preparation, in addition to autonomous healing at 25 °C, temperature-induced healing tests were carried out at 50 and 80 °C. Each experiment was carried out starting from a virgin gel sample. The hydrogels in equilibrium with water were also subjected to healing tests under various healing conditions. The effects of the healing time and healing temperature as well as the treatment of the cut surfaces with acid or surfactant solutions were investigated. For this purpose, the gel samples were cut in the middle, and the cut regions were immersed (5 mm deep) into solutions of various pH's containing CTAB and NaBr for 5–60 min at 35 °C. Then, the two halves were merged together as described above. After repairing, the healed gel samples were transferred into water to remove surfactant and salts of the healing agent.

RESULTS AND DISCUSSION

As described above, we prepared PAAc hydrogels by the micellar copolymerization of AAc with 2 mol % C18 in an aqueous CTAB–NaBr solution. The synthesis parameters varied were (i) the total monomer concentration C_0 and (ii) the molar ratio β_0 of CTAB to AAc monomer in the feed (Table 1). A typical gelation profile of the micellar copolymerization reactions is shown in Figure 2A, where the elastic modulus G', the viscous modulus G'', and the loss factors tan δ (= G''/G') of the reaction system at an angular frequency of 6.3 rad s^{-1} are plotted against the reaction time. The general trend is a rapid increase of the dynamic moduli followed by a plateau regime after a reaction time of about 1 h where the moduli slightly increase. As seen in Figure S2, the plateau elastic modulus G' increases with increasing monomer concentration C_0 or with decreasing CTAB/AAc molar ratio β_0 in the feed. Figure 2B shows the frequency dependencies of G' (filled symbols) and G'' (open symbols) for the gels formed at various C_0 and β_0. The dynamic moduli of the physical gels are frequency dependent over the range of frequency between 0.08 and 400 rad s^{-1}, indicating their elastic and viscous energy dissipating properties. G' slightly increases with rising C_0

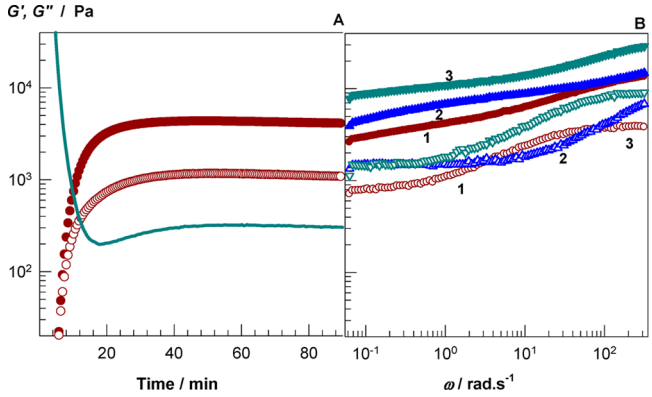

Figure 2. (A) Elastic modulus G' (filled symbols), the viscous modulus G'' (open symbols), and loss factor tan δ (lines) during the micellar copolymerization of AAc with 2 mol % C18 at 50 °C in CTAB–NaBr solution shown as a function of the reaction time. C_0 = 20% w/v, β_0 = 1/8, ω = 6.3 rad s^{-1}, and γ_0 = 0.01. (B) Frequency dependence of G' (filled symbols) and G'' (open symbols) for gels just after their preparation. (1) β_0 = 1/8, C_0 = 20. (2) β_0 = 1/8, C_0 = 30% w/v. (3) β_0 = 1/10, C_0 = 30% w/v. γ_0 = 0.01. Temperature = 25 °C.

because of the increase of the polymer concentration in the hydrogel. G' also increases with decreasing β_0 ratio which is attributed to the strengthening of the hydrophobic interactions between C18 blocks as the surfactant amount in the hydrogel is decreased.[36,61]

All the physical gels formed after a reaction time of 24 h were insoluble in water with a gel fraction close to unity (Table 1), revealing that the monomers AAc and C18 are incorporated completely into the physical network. Figures 3A,B show the relative mass (m_{rel}) of the hydrogels plotted against the swelling time in water. We have to note that the hydrogels synthesized under identical conditions but using an equally charged surfactant (SDS) instead of CTAB significantly swell in water and attains an equilibrium swelling degree $m_{rel,eq}$ of 500 ± 100 (Figure S4). In contrast, present hydrogels deswell in water with 40–60% reduction in the gel mass, indicating the onset of complexation between PAAc and CTAB upon immersion in water. Indeed, polymers isolated from the hydrogels that were in thermodynamic equilibrium with pure water contained 0.9–1.5% nitrogen, indicating the presence of polymer-bound CTAB molecules (Table S2). The amount of bound CTA counterions was calculated between 19 and 30 wt %, corresponding to a molar ratio β of CTAB to the AAc units of the polymer between 0.065 and 0.120, as listed in the third column of Table 1. Thus, on average, 8–15 AAc units of the physical network carry CTA counterions that cannot be extracted with water. The β ratio increases as the CTAB/AAc ratio in the feed (β_0) is increased or, as the initial monomer concentration (C_0) is decreased. The increase in β also leads to a more collapsed state of gels in water, as represented by $m_{rel,eq}$ values in Table 1.

The fact that the onset of complexation between PAAc and CTAB occurs after immersion of the hydrogels in water was also obvious from the inspection of the gel samples. Photographs of typical PAAc hydrogels in the form of rods and spheres after preparation (a) and in equilibrium with water (b) are shown in Figure 3C. All the physical hydrogels that were transparent after preparation became opaque in water, indicating formation of a two-phase structure, and the opacity increased as the β ratio increases. These observations are similar

dx.doi.org/10.1021/ma5015116 | Macromolecules 2014, 47, 6889–6899

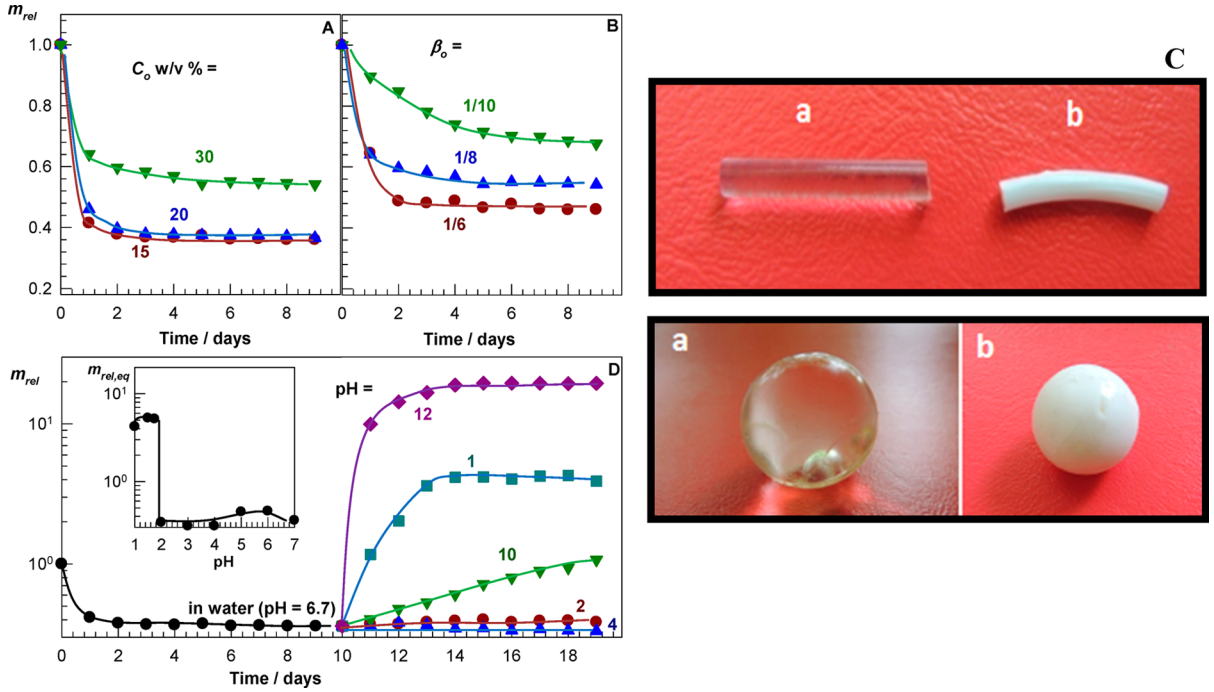

Figure 3. (A, B) Relative mass m_{rel} of the physical gels formed at β_0 = 1/8 (A) and C_0 = 30% (B) plotted against the swelling time in water. (C) Photographs of PAAc hydrogels formed at C_0 = 20%. β_0 = 1/8 after preparation (a) and in equilibrium with water (b). (D) m_{rel} vs swelling time plot for the physical gel prepared at C_0 = 15% and β_0 = 1/8. After equilibrium in water, the gel was immersed in aqueous solutions of various pH's indicated. The inset represents the equilibrium values of m_{rel} ($m_{rel,eq}$) plotted against the pH of the external solution.

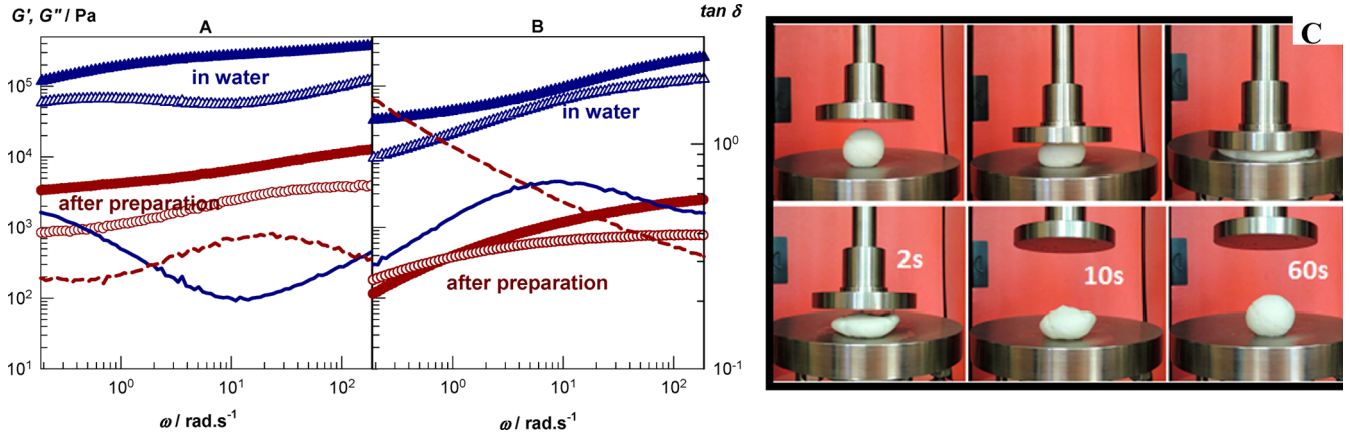

Figure 4. (A, B) Frequency dependence of G' (filled symbols), G'' (open symbols), and tan δ (curves) for gels formed at C_0 = 20% w/v and β_0 = 1/8 with (A) and without the hydrophobe C18 (B). Measurements were performed both after gel preparation (circles, dashed curves) and in equilibrium with water (triangles, solid curves). γ_0 = 0.01. Temperature = 25 °C. (C) Photographs of a PAAc hydrogel sphere during compression (upper panel) and at various times after unloading (bottom panel). C_0 = 20% and β_0 = 1/8.

to those reported previously for aqueous solutions containing PAAc and CTAB.[42] At certain compositions, such systems can separate into a concentrated turbid phase and a transparent dilute phase.[42] Figure 3D shows the swelling curves of a gel sample formed at C_0 = 15% and β_0 = 1/8. The gel is first immersed in water up to 10 days followed in aqueous solutions of various pH's. Transferring the collapsed gel from water (pH = 6.7) into acidic or basic solutions results in gel swelling. Swelling in basic solutions is due to the ionization of AAc units,[49] while in acidic solutions of pH < 2 due to the un-ionized form of PAAc chains leading to the dissociation of PAAc/CTAB complex. The inset in Figure 3D showing the equilibrium mass $m_{rel,eq}$ of gels in aqueous solutions of pH between 1 and 7 indicates that the collapsed gel reswells in acidic solutions of pH < 2. This confirms that complexation did not occur at the state of gel preparation at which pH inside the gel is equal to 1.5.

Figure 4A shows the typical mechanical spectrum of PAAc hydrogel in equilibrium with water. For comparison, the spectrum of the same gel after synthesis is also given in the figure. The dynamic moduli of the hydrogel increase by 1 order of magnitude upon immersion in water, suggesting the effect of complex formation between PAAc with CTA counterions. Further, both moduli of the gel are still frequency dependent and tan δ remains above 0.1 after equilibrium in water, i.e., after extraction of free CTAB micelles. This behavior emphasizes viscous character of PAAc hydrogels in water environment, which is in strong contrast to the self-healing hydrogels forming

dx.doi.org/10.1021/ma5015116 | Macromolecules 2014, 47, 6889−6899

no complex with surfactants.[36,61] For instance, PAAm hydrogels prepared with 2 mol % C18 in SDS solutions show frequency-independent elastic modulus after swelling in water and, the loss factor decreases from 0.2 to below 0.1 due to the strong hydrophobic associations between the blocks of C18 units in the absence of surfactant.[36,61] The viscoelastic behavior of present hydrogels in equilibrium with water is illustrated by the photographs in Figure 4C. PAAc gel sphere can be compressed more than 90% without any crack development. After the release of the load, the gel reverts back to close to the original dimensions within 60 s.

The viscoelastic behavior of the hydrogels in equilibrium with water suggests that the aggregates of CTA counterions within the gel contribute to the dynamics of the associations between the hydrophobic blocks. To highlight the effect of polymer-bound CTA counterions on the dynamics of gels, we prepared a reference physical PAAc gel in CTAB−NaBr solution without using the hydrophobic monomer C18. In such a hydrogel, hydrophobic associations between C18 blocks do not exist so that the effect of surfactant alkyl counterions could be visualized. At the preparation state, the reference gel was transparent as the hydrophobically modified ones, while it became opaque after immersion in water with 30% reduction in the water content, indicating the onset of complexation due to the increased pH from 1.5 to 6.7. Indeed, the molar ratio β of CTAB-to-AAc units of the polymer isolated from the reference gel was 1/11. Figure 4B shows the mechanical spectra of the reference gel after preparation and after equilibrium with water. After preparation (circles and dashed curve), the transparent gel exhibits a liquid-like response typical for a semidilute polymer solution; i.e., G'' exceeds G' at low frequencies while there is a crossover between G' and G'' at ω = 0.8 s^{-1}. After immersion in water (triangles and solid curve), the crossover frequency shifts outside of the experimental window, and the dynamic moduli of the gel increase by 2 orders of magnitude due to the formation of the PAAc−CTAB complex. Thus, despite the lack of the hydrophobic blocks in the polymer backbone, physical gels consisting of PAAc chains with CTA counterions could be obtained that were stable in water. Note that when CTAB is replaced with an equally charged surfactant such as SDS during the preparation of the reference gel, it becomes soluble in water. Thus, micellization of polymer-bound CTA counterions in the semidilute PAAc solution is responsible for the formation of the reference gel, as also reported in the literature.[48] Comparing Figures 4A and 4B, we can conclude that the present gels containing hydrophobic C18 blocks have two types of physical cross-links depending on which state they are. The first type exists at the preparation state of gels and includes hydrophobic associations between C18 blocks weakened by CTAB micelles. The second type appears after immersion of the hydrogels in water and includes the aggregates of polymer-bound CTA counterions and alkyl groups of C18 blocks. The second type of cross-links is responsible for the drastic increase in the dynamic moduli and for the preservation of viscous, energy dissipating properties of PAAc hydrogels in equilibrium with water.

To highlight the effect of polymer-bound CTA counterions on the mechanical properties of hydrogels, cylindrical gel samples after a reaction time of 24 h were subjected to uniaxial elongation and compression tests. Figure 5 represents stress−strain data of the physical gels after preparation (dashed curves) and in equilibrium with water (solid curves), as the dependence of the nominal stress σ_{nom} on the deformation ratio λ. The

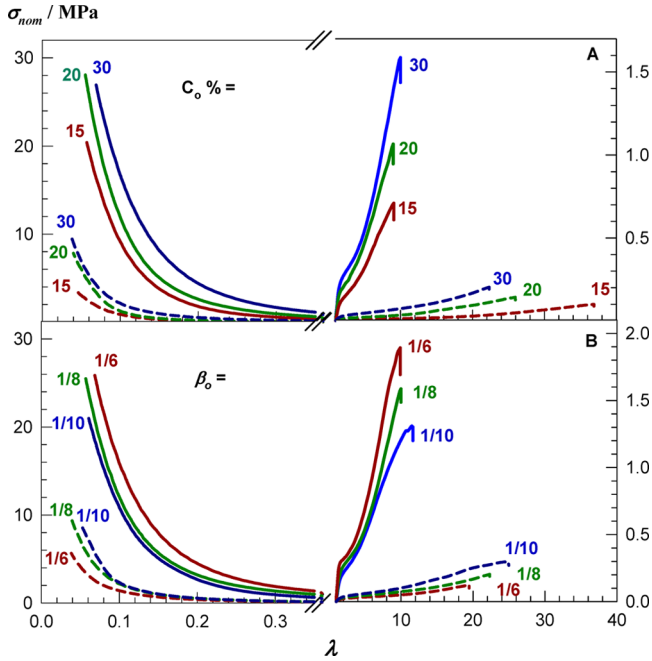

Figure 5. Stress−strain curves of the physical gels after preparation (dashed curves) and in equilibrium with water (solid curves) under compression (λ < 1) and elongation (λ > 1) as the dependence of nominal stress σ_{nom} on the deformation ratio λ. Synthesis parameters: (A) β_0 = 1/8 and C_0 % w/v as indicated. (B) C_0 = 30% w/v and β_0 as indicated.

characteristic tensile and compression data of the gels, i.e., the Young's modulus E, the fracture stress σ_f, and stretch at break λ_f, are collected in Table 1 and Table S1. A significant enhancement in the mechanical properties of hydrogels is observable upon their immersion in water. For instance, 20-fold increase in the modulus E and 14-fold increase in the fracture stress σ_f were observed after swelling of the hydrogel formed at C_0 = 30% w/v and β_0 = 1/6. The largest modulus and the fracture stress are 605 ± 20 kPa and 1.66 ± 0.24 MPa, respectively, which were obtained at the highest β ratio of 1/8.3. Such a drastic change in the mechanical properties of gels upon their immersion in water is attributed to the extraction of CTA counterions from the micelles by AAc anions and simultaneous formation of ionic bonds at neutral pH.

The variations of the modulus and the tensile strength of gels formed at various β_0 ratios also support this explanation (Table 1). At a fixed monomer concentration C_0, increasing CTAB content (β_0) in the feed slightly decreases the modulus E and the fracture stress σ_f of the gels at the state of their preparation. This is expected due to the weakening of the hydrophobic interactions in the presence of free surfactant micelles.[36] However, upon immersion in water, the larger the ratio β_0, the larger is the amount of bound CTAB (β) and the larger is the modulus and the fracture stress. This highlights significant effect of the CTA counterions on the mechanical properties of the hydrogels. Similar results were also observed by the compression tests (Table S1). The drastic increase of the modulus with rising amount of bound CTAB is attributed to the formation of larger number of mixed micelles consisting of CTA counterions and C18 blocks. A similar behavior was reported before in aqueous solutions of hydrophobically modified PAAc (1%).[48] The viscosity η of such solutions increases with increasing concentration of the cationic

dx.doi.org/10.1021/ma5015116 | Macromolecules 2014, 47, 6889−6899

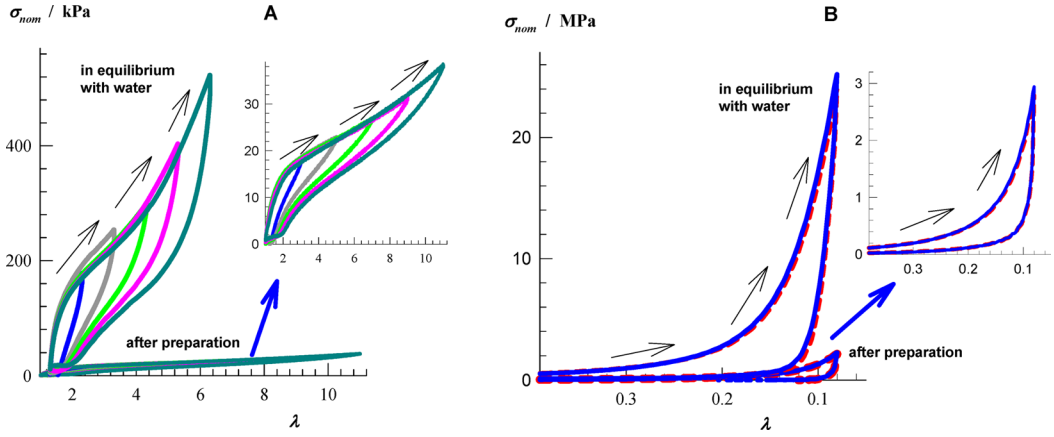

Figure 6. σ_{nom} vs λ curves from cyclic tensile (A) and compression tests (B) for gels after preparation and in equilibrium with water. C_0 = 20% and β_0 = 1/8. (A) Five successive loading/unloading cycles with increasing maximum strain λ_{max}. (B) Two successive loading/unloading cycles up to λ_{max} = 0.08.

surfactant dodecyltrimethylammonium bromide (DTAB). At surfactant concentrations above 10^{-4} M, η exponentially increases with rising amount of DTAB in the solution, and finally an elastic gel forms between 10^{-3} and 10^{-2} M DTAB.[48]

The nature of the physical cross-links in the hydrogels was compared by cyclic compression and elongation tests. The tests were conducted by compression or stretching of cylindrical gel samples at a constant cross-head speed to a predetermined maximum strain λ_{max}, followed by immediate retraction to zero displacement. After a fixed waiting time of 5 min, the cycles were repeated several times. Figure 6A shows the results of five successive tensile loading/unloading cycles with increasing λ_{max} for the gel formed at C_0 = 20% and β_0 = 1/8. For the same gel sample, two successive compressive cycles up to λ_{max} = 0.08 (92% compression) are shown in Figure 6B. In all cases, the loading curve of the cycle was different from the unloading curve, indicating damage in the gels and dissipation of energy during the cycle. However, the loading curve of each cycle follows that of the previous cycle indicating that the behavior of virgin gel sample can be recovered when the sample is left to rest for 5 min without stress. Figure 6A also shows that the unloading curves do not return to zero strain after the cycle. Visual observations showed that the residual deformation after the cycle decreased with increasing waiting time and disappeared after 5 min, so that the next loading curve follows the path of the previous one. The reversibility of loading/unloading cycles was observed in all gels listed in Table 1, both at the state of preparation and at equilibrium in water (Figure 6 and Figure S5). The good superposition of the successive loading curves demonstrates that the damage done to the gel samples during the loading cycle is recoverable in nature. Therefore, the energy U_{hys} dissipated during the mechanical cycles is proportional to the number of reversibly breakable cross-links in the hydrogels.[36,62]

The hysteresis energies U_{hys} were calculated from the area between the loading and unloading curves shown in Figure 6. They are plotted in Figure 7 against λ_{max} and C_0. Increasing maximum strain λ_{max} or increasing C_0, that is, PAAc concentration, in the hydrogel also increases the hysteresis energy U_{hys} due to the simultaneous increase in the number of breakable bonds. The overlap U_{hys} vs C_0 plots in Figure 7B obtained from two successive compression tests up to 92% deformation show total recovery of the original microstructure of gels both after preparation and after equilibrium in water.

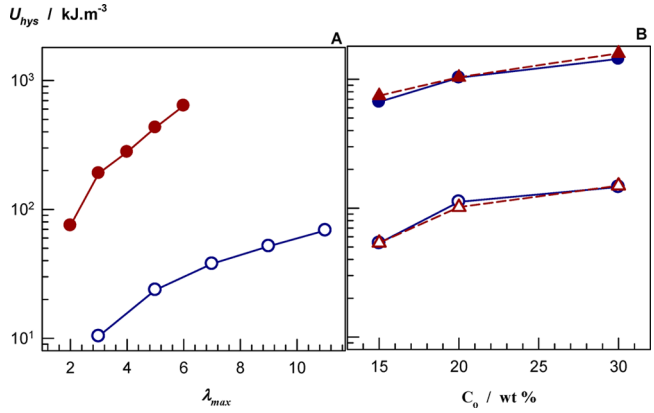

Figure 7. (A) Hysteresis energy U_{hys} of gels during successive tensile loading/unloading cycles plotted against λ_{max}. C_0 = 20% and β_0 = 1/8. (B) U_{hys} of gels during two successive compressive cycles up to λ_{max} = 0.08 plotted against C_0. Filled and open symbols represent data obtained from gels after equilibrium in water and after preparation, respectively.

Further, U_{hys} of gels in equilibrium with water is about 1 order of magnitude larger than that of the gels after preparation, indicating formation of larger number of reversibly breakable cross-links upon gel swelling. This is in contrast to the nonionic hydrogels formed via hydrophobic associations.[36,61] In these gels, although the loading curve of the first cycle is different from the unloading, the following cycles are almost elastic due to the occurrence of an irrecoverable damage to the gel sample during the first cycle. In contrast, present gels both at the state of preparation and in equilibrium with water show reversible cycles with increased degree of hysteresis upon swelling.

Reversible disengagements of the associations under an external force point out the self-healing behavior of the hydrogels. This was indeed observed in gels at the state of preparation and at equilibrium in water. To quantify the healing efficiency, tensile testing experiments were performed using virgin and healed cylindrical gel samples. For the hydrogels at the preparation state, autonomic self-healing was observed within a time period of a few minutes. In Figure 8A, stress–strain curves of the virgin and healed gel samples formed at various C_0 and at the state of their preparations are shown for a healing time of 30 min and for two different healing temperatures. At 25 °C, a complete recovery of the initial

dx.doi.org/10.1021/ma5015116 | Macromolecules 2014, 47, 6889–6899

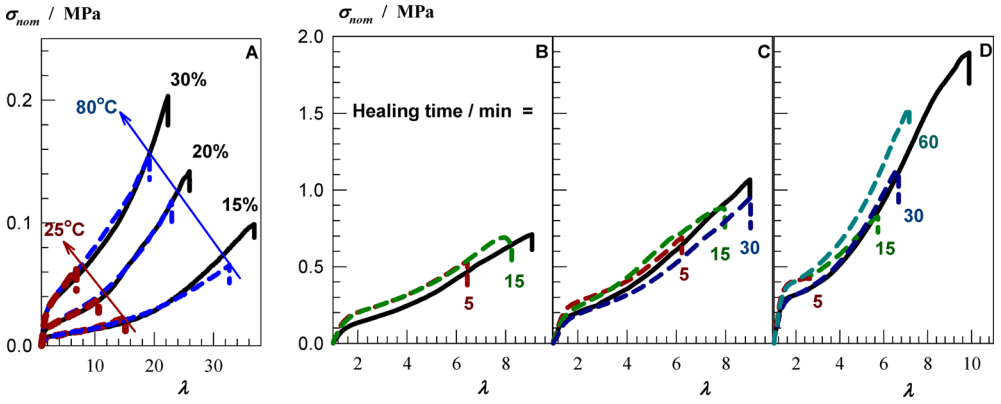

Figure 8. Stress−strain curves of virgin (solid curves) and healed gel samples (dashed curves). (A) PAAc hydrogels after preparation state formed at $\beta_0 = 1/8$ and at various C_0 indicated. Healing time = 30 min. Healing temperature: 25 °C (dark red curves) and 80 °C (blue curves). (B−D) PAAc hydrogels in equilibrium with water: (B) $C_0 = 15\%$, $\beta_0 = 1/8$; (C) $C_0 = 20\%$, $\beta_0 = 1/8$; (D) $C_0 = 30\%$, $\beta_0 = 1/6$.

modulus E was observed while the healing efficiency with respect to the fracture stress was between 20 and 30%. Healing efficiency increases with increasing temperature during healing (Figure 8A). For instance, the efficiencies are 30 and 75% at 25 and 80 °C, respectively, for the hydrogel formed at $C_0 = 30\%$. The highest fracture stress of the hydrogels self-healed at 80 °C is 0.16 MPa.

High-strength PAAc hydrogels in equilibrium with water were also subjected to healing tests under various healing conditions. Although autonomic self-healing was not observed, increasing the healing temperature to 80 °C induced healing within 30−60 min (Figure S6). The treatment of the cut surfaces with acid or surfactant solutions before heating to 80 °C further increased the healing efficiency (Figure S6). The highest healing efficiencies were achieved when the cut surfaces were treated at 35 °C with CTAB (10%)−NaBr (0.25 M) solutions of pH = 1, which provided complete dissolution of PAAc−CTAB complex in the damaged area. After repairing the gel samples, the welded interface acted as a weak point in the healed gels due to the presence of surfactant so that they always ruptured at this region. Therefore, the healed gel samples were immersed in water to extract the healing agent before the mechanical tests. The photographs in Figure 9 show healing of ruptured gel samples in equilibrium with water. The joint re-formed between cut surfaces withstands large external stresses as the original gel sample before its fracture. In Figures 8B−D, stress−strain curves of the virgin and healed gel samples in equilibrium with water are shown for various healing times in surfactant solutions. The fracture stress of healed gels increases with increasing healing time or with decreasing PAAc concentration of the hydrogels. For instance, after a healing time of 30 min, almost complete healing was achieved in the hydrogels formed at $C_0 = 20\%$ (Figure 8C), while increasing C_0 to 30% decreases the healing efficiency to 50%. After a healing time of 60 min, the hydrogel sample formed at $C_0 = 30\%$ and $\beta_0 = 1/6$ sustains 1.5 ± 0.2 MPa stresses and ruptures at a stretch of 7 ± 1 (Figure 8D). To our knowledge, this fracture stress is the highest value reported so far in the literature.

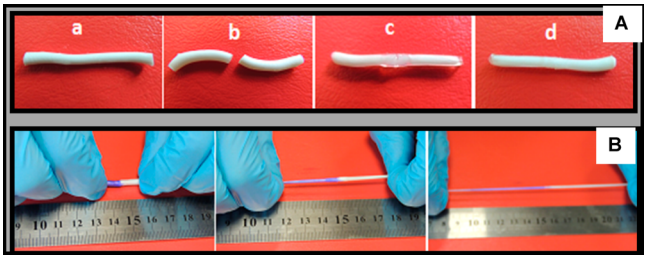

Figure 9. Healing of PAAc hydrogel samples, in equilibrium with water, formed at $C_0 = 30\%$ and $\beta_0 = 1/6$. Healing agent: CTAB (10%)−NaBr (0.25 M) solution at pH = 1. (A) Photographs before (a) and after cutting of the sample into two pieces (b). After the treatment of cut surfaces with the surfactant solution and pressing them together (c), they merge into a single piece (d). (B) Photographs during stretching of a hydrogel sample self-healed via heating and surfactant treatment. One of the virgin samples forming the healed gel is colored with crystal violet for clarity.

As mentioned above, the damage created in the hydrogels is much better healed by storing the gel samples at an elevated temperature. To understand the underlying mechanism of temperature-triggered healing in PAAc hydrogels, we monitored the dynamic moduli of gels as a function of temperature. Both moduli of the gel samples rapidly decreased as the temperature is increased, indicating that the gel becomes weak with rising temperature (Figure S7). The decrease of the dynamic moduli upon increase of temperature was already observed in semidilute solutions of hydrophobically modified PAAm's.[51,63] This behavior can be ascribed to increased solubility of hydrophobic moieties in aqueous solutions leading to a decrease in the association degree of polymers.[51] Thus, increasing ability of the hydrogels to self-heal at a high temperature is due to the simultaneous increase of the chain mobility so that the polymer chains on the two cut surfaces can easily diffuse from one side to the other, and the hydrophobes across the rupture interface become more accessible to each other.

We observed that the variation of the modulus with temperature is strongly dependent on the water contents, w_{H_2O}, of the hydrogels. In Figure 10A, the elastic modulus G' of PAAc hydrogel formed at $C_0 = 20\%$ and $\beta_0 = 1/8$ is plotted against the temperature. The hydrogel contains various amounts of water w_{H_2O}, as indicated in the figure. At 20 °C, G' of the equilibrium swollen gel sample containing 40% water amounts to 60 kPa, while it substantially increases to 8.7 MPa when w_{H_2O} is reduced to 12%. Upon heating to 80 °C, about 2- and 8-fold decrease in G' were observed for the gel at $w_{H_2O} = 40$ and 12%, respectively. In Figure 10B, the variations of G' and tan δ of hydrogels at 12 and 16% water contents are shown

dx.doi.org/10.1021/ma5015116 | Macromolecules 2014, 47, 6889−6899

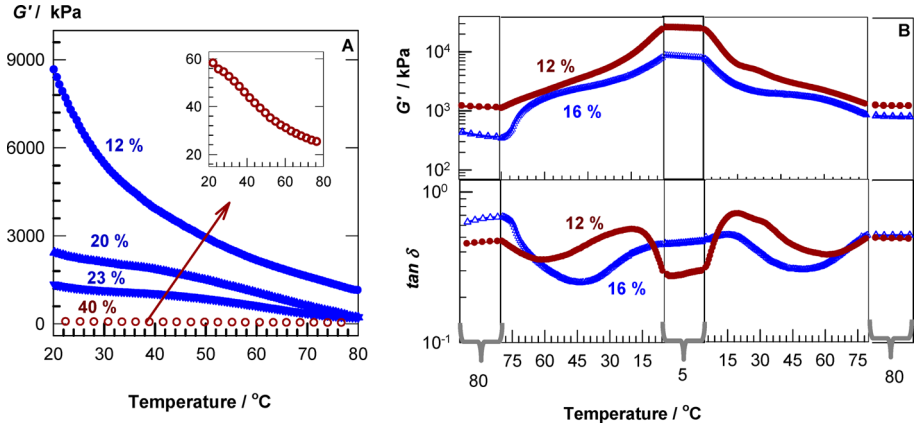

Figure 10. (A) Elastic modulus G' of PAAc hydrogels shown as a function of the temperature. (B) Viscoelastic behavior of PAAc hydrogels during the cooling–heating cycle between 80 and 5 °C. C_0 = 20% and β_0 = 1/8. The water contents (w_{H_2O}) are indicated. ω = 6.28 rad s^{-1} and γ_0 = 0.001.

during the cooling–heating cycle between 80 and 5 °C. The gels undergo an almost reversible 20-fold change in the elastic modulus between 80 and 5 °C, i.e., between 8–26 and 0.4–1 MPa. Such a large difference in the modulus between high and low temperatures is the most significant factor to induce the shape memory effect.[64−68]

Figure 11A and the movie attached as Supporting Information demonstrate shape memory behavior of a PAAc hydrogel sample at w_{H_2O} = 12%. The permanent shape of the sample is İTÜ, the abbreviated name of our university (a). After heating to 70 °C, the gel become soft and could easily be deformed into a temporary shape (b). This temporary shape was fixed by cooling the sample to 25 °C. After immersing the gel sample in a water bath at 70 °C (c → e), it returned back to its initial shape within 10 s. All hydrogel samples in equilibrium with water or at a water content as low as 10% exhibited 100% shape-recovery ratios at 70 °C, as determined by the bending tests described before.[68]

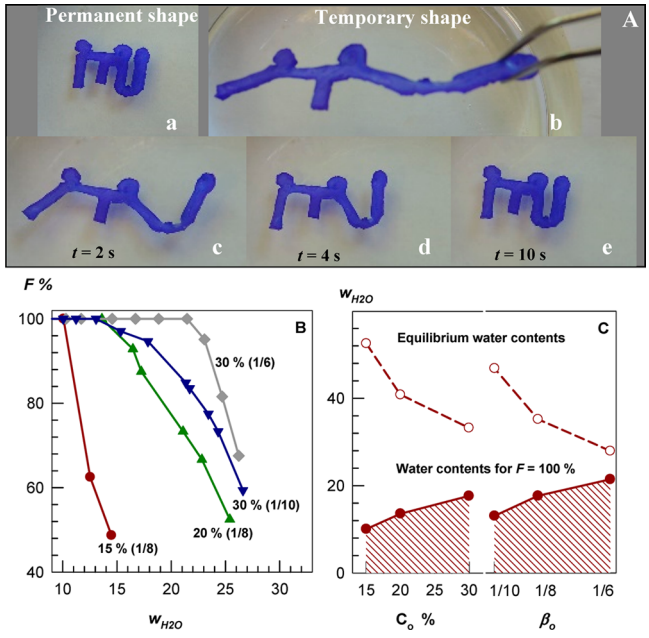

Figure 11. (A) Images of permanent (a) and temporary shapes (b) of a hydrogel sample at w_{H_2O} = 12% and the transition from the temporary shape to the permanent shape (b → e). The recovery takes 10 s after immersing the gel sample in a water bath at 70 °C. C_0 = 20% and β_0 = 1/8. (B) Shape-fixing efficiency F of hydrogels plotted against their water contents w_{H_2O}. Synthesis parameters of the hydrogels (C_0 and β_0, in parentheses) are indicated. (C) Equilibrium water content (open symbols) and the critical water content for F = 100% (filled symbols) plotted against C_0 and β_0. The dashed area represents the water amount in hydrogels required for 100% fixing efficiency.

To determine shape-fixing efficiency, cylindrical gel samples were immersed in a water bath at 70 °C. The gels that became soft were stretched at 70 °C to twice their original lengths. Then, the temporary shapes were fixed by immersing the gel samples in a water bath at 25 °C for 1 min. The shape-fixing efficiency F representing the ability of the gel sample to hold its temporary shape was calculated as[67] $F = (l_t - l_0)/(l_s - l_0)$, where l_0 and l_s are the initial and stretched lengths of the gel sample, and l_t is its length after a fixing time t = 1 min at 25 °C. In Figure 11B, F is plotted against the water content w_{H_2O} of the hydrogels. A complete fixing efficiency is observable if w_{H_2O} of the gel samples is reduced below a critical value. For instance, the gel formed at C_0 = 30% and β_0 = 1/6 containing 28% water at equilibrium state exhibits 100% fixing efficiency if its water content is reduced below 20%. In Figure 11C, the equilibrium water content (open symbols) and the critical water content for 100% fixing efficiency (filled symbols) are plotted against C_0 and β_0. The dashed area represents the water amount in gels required for 100% fixing efficiencies. The equilibrium water content of the hydrogels decreases with rising C_0 or β_0 due to the simultaneously increase of Young's modulus, i.e., the effective cross-link density of the supramolecular network (Table 1). This leads to generation of stronger shape memory effect over a wider range of water concentration.

DSC measurements conducted between 5 and 80 °C revealed that the hydrogels at various w_{H_2O}, including the completely dried ones, have no crystalline domains. In the shape memory hydrogels reported by Osada et al.[64−66] and Bilici et al.,[68] the alkyl side chains are in a crystalline state after cooling below the transition temperature so that the deformed shapes can easily be fixed. In the present hydrogels, since alkyl side chains are in noncrystalline state even at 5 °C, hydrophobic associations between C18 blocks and CTA counterions cannot support the residual stress in PAAc network chains so that the fixation ability is low. A complete fixing efficiency thus requires strengthening of the associations by

dx.doi.org/10.1021/ma5015116 | Macromolecules 2014, 47, 6889–6899

decreasing the water amount in the hydrogels. This shape memory mechanism was also confirmed by the temperature dependent variation of the elastic modulus G' of hydrogels (Figure 10B). While hydrogels containing crystalline domains exhibit drastic changes in G' in a narrow range of temperature corresponding to the transition temperature,[68] G' of present hydrogels gradually changes with a change in temperature. Thus, although the shape fixation ability of PAAc hydrogels is not good as those containing crystalline domains, they can recover to a desired shape by controlling the recovery temperature which determines the strength of hydrophobic associations.

CONCLUSIONS

A promising strategy to design synthetic hydrogels with the ability to self-heal is to substitute the covalently cross-linked polymer chains by supramolecular ones. Although supramolecular hydrogels generally exhibit rapid self-healing without the need for any stimulus or healing agent, they suffer from low mechanical strength which prevents them from any stress-bearing applications. In the present work, we described a novel way for the production of self-healing hydrogels with shape memory behavior of high tensile strength (0.7−1.7 MPa) and stretch at break (800−900%). Hydrophobically modified PAAc chains with CTA counterions form the physical network of such hydrogels. The hydrogels were prepared via micellar copolymerization of AAc with 2 mol % C18 as the hydrophobic comonomer in aqueous CTAB solutions. The solubility of the large hydrophobe C18 in CTAB solution was provided by the addition of NaBr (0.25 M), which causes CTAB micelles to grow and thus solubilize C18 within the grown micelles. Extraction of free CTAB micelles from the physical gels results in a drastic increase in their Young's moduli (from 8−30 to 180−600 kPa) and tensile strengths (from 0.1−0.2 to 0.7−1.7 MPa) due to the complex formation between PAAc and CTAB. Loading and unloading cycles conducted on hydrogels after synthesis and after equilibrium in water show a significant hysteresis and good superposition of the successive loading curves, demonstrating damage done during loading is recoverable in nature. The hydrogel samples self-healed via heating and surfactant treatment of the damaged areas withstand up to 1.5 MPa stresses and rupture at a stretch of 600%. Because of the drastic change in the elastic modulus of PAAc hydrogels with a change in temperature, they also exhibit shape memory properties with a recovery ratio of 100%.

ASSOCIATED CONTENT

Supporting Information

Table S1, compressive mechanical properties of PAAc hydrogels; Table S2, elemental analysis results of dried polymers; Figure S1, ξ of the gelation solutions; Figure S2, dynamic moduli vs reaction time plots; Figure S3, stress−strain curves of the hydrogels; Figure S4, photographs of PAAc hydrogels formed using SDS; Figure S5, cyclic compression test results; Figure S6, stress−strain curves of virgin and healed gel samples; Figure S7, temperature dependence of the dynamic moduli of hydrogels; movie demonstrating the shape memory behavior of the hydrogels. This material is available free of charge via the Internet at http://pubs.acs.org.

AUTHOR INFORMATION

Corresponding Author

*E-mail okayo@itu.edu.tr (O.O.).

Notes

The authors declare no competing financial interest.

ACKNOWLEDGMENTS

Work was supported by the Scientific and Technical Research Council of Turkey (TUBITAK), KBAG 114Z312. O.O. thanks Turkish Academy of Sciences (TUBA) for the partial support.

REFERENCES

(1) Fratzl, P. *J. R. Soc. Interface* **2007**, *4*, 637.
(2) Amendola, V.; Meneghetti, M. *Nanoscale* **2009**, *1*, 74.
(3) Fantner, G. E.; Oroudjev, E.; Schitter, G.; Golde, L. S.; Thurner, P.; Finch, M. M.; Turner, P.; Gutsmann, T.; Morse, D. E.; Hansma, H.; Hansma, P. K. *Biophys. J.* **2006**, *90*, 1411.
(4) Annable, T.; Buscall, R.; Ettelaie, R.; Whittlestone, D. *J. Rheol.* **1993**, *37*, 695.
(5) Lehn, J.-M. *Proc. Natl. Acad. Sci. U. S. A.* **2002**, *99*, 4763.
(6) Cordier, P.; Tournilhac, F.; Souli-Ziakovic, C.; Leibler, L. *Nature* **2008**, *451*, 977.
(7) Xu, D.; Craig, S. L. *Macromolecules* **2011**, *44*, 5465.
(8) Seiffert, S.; Sprakel, J. *Chem. Soc. Rev.* **2012**, *41*, 909.
(9) Guimard, N. K.; Oehlenschlaeger, K. K.; Zhou, J.; Hif, S.; Schmidt, F. G.; Barner-Kowollik, C. *Macromol. Chem. Phys.* **2012**, *213*, 131.
(10) Hager, M. D.; Greil, P.; Leyens, C.; van der Zwaag, S.; Schubert, U. S. *Adv. Mater.* **2010**, *22*, 5424.
(11) Wu, D. Y.; Meure, S.; Solomon, D. *Prog. Polym. Sci.* **2008**, *33*, 479.
(12) Brochu, A. B. W.; Craig, S. L.; Reichert, W. M. *J. Biomed. Mater. Res., Part A* **2011**, *96*, 492.
(13) Zhao, Y.; Sakai, F.; Su, L.; Liu, Y.; Wei, K.; Chen, G.; Jiang, M. *Adv. Mater.* **2013**, *25*, 2515.
(14) Peak, C. W.; Wilker, J. J.; Schmidt, G. *Colloid Polym. Sci.* **2013**, *291*, 2031.
(15) Phadke, A.; Zhang, C.; Arman, B.; Hsu, C.-C.; Mashelkar, A.; Lele, A. K.; Tauber, M. J.; Arya, G.; Varghese, S. *Proc. Natl. Acad. Sci. U. S. A.* **2012**, *109*, 4383.
(16) Zhang, H.; Xia, H.; Zhao, Y. *ACS Macro Lett.* **2012**, *1*, 1233.
(17) Cui, J.; del Campo, A. *Chem. Commun.* **2012**, *48*, 9302.
(18) Liu, J.; Song, G.; He, C.; Wang, H. *Macromol. Rapid Commun.* **2013**, *34*, 1002.
(19) Haraguchi, K.; Uyama, K.; Tanimoto, H. *Macromol. Rapid Commun.* **2011**, *32*, 1253.
(20) South, A. B.; Lyon, L. A. *Angew. Chem., Int. Ed.* **2010**, *49*, 767.
(21) Wang, Q.; Mynar, J. L.; Yoshida, M.; Lee, E.; Lee, M.; Okura, K.; Kinbara, K.; Aida, T. *Nature* **2010**, *463*, 339.
(22) Sun, J.-Y.; Zhao, X.; Illeperuma, W. R. K.; Chaudhuri, O.; Oh, K. H.; Money, D. J.; Vlassak, J. J.; Suo, Z. *Nature* **2012**, *489*, 133.
(23) Foo, C. T. S. W. P.; Lee, J. S.; Mulyasasmita, W.; Parisi-Amon, A.; Heilshorn, S. C. *Proc. Natl. Acad. Sci. U. S. A.* **2009**, *106*, 22067.
(24) Appel, E. A.; Biedermann, F.; Rauwald, U.; Jones, S. T.; Zayed, J. M.; Scherman, O. A. *J. Am. Chem. Soc.* **2010**, *132*, 14251.
(25) Skrzeszewska, P. J.; Sprakel, J.; Wolf, F. A.; Fokkink, R.; Stuart, M. A. C.; van de Gucht, J. *Macromolecules* **2010**, *43*, 3542.
(26) Holten-Andersen, N.; Harrington, M. J.; Birkedal, H.; Lee, B. P.; Messersmith, P. B.; Lee, K. Y. C.; Waite, J. H. *Proc. Natl. Acad. Sci. U. S. A.* **2011**, *108*, 2651.
(27) Shafiq, Z.; Cui, J.; Pastor-Perez, L.; San Miguel, V.; Gropeanu, R. A.; Serrano, C.; del Campo, A. *Angew. Chem., Int. Ed.* **2012**, *124*, 4408.
(28) Xu, Y.; Wu, Q.; Sun, Y.; Bai, H.; Shi, G. *ACS Nano* **2010**, *4*, 7358.
(29) Liu, F.; Li, F.; Deng, G.; Chen, Y.; Zhang, B.; Zhang, J.; Liu, C.-Y. *Macromolecules* **2012**, *45*, 1636.
(30) Deng, G.; Tang, C.; Li, F.; Jiang, H.; Chen, Y. *Macromolecules* **2010**, *43*, 1191.
(31) Zhang, Y.; Tao, L.; Li, S.; Wei, Y. *Biomacromolecules* **2011**, *12*, 2894.

(32) He, L.; Fullenkamp, D. E.; Rivera, J. G.; Messersmith, P. B. *Chem. Commun.* **2011**, *47*, 7497.
(33) Froimowicz, P.; Klinger, D.; Landfester, K. *Chem.—Eur. J.* **2011**, *17*, 12465.
(34) Quint, S. B.; Pacholski, C. *Soft Matter* **2011**, *7*, 3735.
(35) Tuncaboylu, D. C.; Sari, M.; Oppermann, W.; Okay, O. *Macromolecules* **2011**, *44*, 4997.
(36) Tuncaboylu, D. C.; Sahin, M.; Argun, A.; Oppermann, W.; Okay, O. *Macromolecules* **2012**, *45*, 1991.
(37) Gulyuz, U.; Okay, O. *Soft Matter* **2013**, *9*, 10287.
(38) Hao, J.; Weiss, R. A. *Macromolecules* **2011**, *44*, 9390.
(39) Hao, X.; Liu, H.; Lu, Z.; Xie, Y.; Yang, H. *J. Mater. Chem. A* **2013**, *1*, 6920.
(40) Lim, P. F. C.; Chee, L. Y.; Chen, S. B.; Chen, B.-H. *J. Phys. Chem. B* **2003**, *107*, 6491.
(41) Yoshida, K.; Dubin, P. L. *Colloids Surf., A* **1999**, *147*, 161.
(42) Ilekti, P.; Piculell, L.; Tournilhac, F.; Cabane, B. *J. Phys. Chem. B* **1998**, *102*, 344.
(43) Fundin, J.; Hansson, P.; Brown, W.; Lidegran, I. *Macromolecules* **1997**, *30*, 1118.
(44) Carnali, J. O. *Langmuir* **1993**, *9*, 2933.
(45) Chiappisi, L.; Hoffmann, I.; Gradzielski, M. *Soft Matter* **2013**, *9*, 3896.
(46) Hansson, P. *Langmuir* **1998**, *14*, 2269.
(47) Wang, C.; Tam, K. C. *Langmuir* **2002**, *18*, 6484.
(48) Magny, B.; Iliopoulos, I.; Zana, R.; Audebert, R. *Langmuir* **1994**, *10*, 3180.
(49) Philippova, O. E.; Hourdet, D.; Audebert, R.; Khokhlov, A. R. *Macromolecules* **1996**, *29*, 2822.
(50) Candau, F.; Selb, J. *Adv. Colloid Interface Sci.* **1999**, *79*, 149.
(51) Volpert, E.; Selb, J.; Candau, F. *Polymer* **1998**, *39*, 1025.
(52) Hill, A.; Candau, F.; Selb, J. *Macromolecules* **1993**, *26*, 4521.
(53) Regalado, E. J.; Selb, J.; Candau, F. *Macromolecules* **1999**, *32*, 8580.
(54) Candau, F.; Regalado, E. J.; Selb, J. *Macromolecules* **1998**, *31*, 5550.
(55) Kujawa, P.; Audibert-Hayet, A.; Selb, J.; Candau, F. *J. Polym. Sci., Part B: Polym. Phys.* **2004**, *42*, 1640.
(56) Imae, T.; Ikeda, S. *Colloid Polym. Sci.* **1987**, *265*, 1090.
(57) Magid, L. J. *J. Phys. Chem. B* **1998**, *102*, 4064.
(58) Yazici, I.; Okay, O. *Polymer* **2005**, *46*, 2595.
(59) Gundogan, N.; Melekaslan, D.; Okay, O. *Macromolecules* **2002**, *35*, 5616.
(60) Tuncaboylu, D. C.; Argun, A.; Algi, M. P.; Okay, O. *Polymer* **2013**, *54*, 6381.
(61) Tuncaboylu, D. C.; Argun, A.; Sahin, M.; Sari, M.; Okay, O. *Polymer* **2012**, *53*, 5513.
(62) Webber, R. E.; Creton, C.; Brown, H. R.; Gong, J. P. *Macromolecules* **2007**, *40*, 2919.
(63) Biggs, S.; Selb, J.; Candau, F. *Polymer* **1993**, *34*, 580.
(64) Matsuda, A.; Sato, J.; Yasunaga, H.; Osada, Y. *Macromolecules* **1994**, *27*, 7695.
(65) Osada, Y.; Matsuda, A. *Nature* **1995**, *376*, 219.
(66) Tanaka, Y.; Kagami, Y.; Matsuda, A.; Osada, Y. *Macromolecules* **1995**, *28*, 2574.
(67) Hao, J.; Weiss, R. A. *ACS Macro Lett.* **2013**, *2*, 86.
(68) Bilici, C.; Okay, O. *Macromolecules* **2013**, *46*, 3125.